Structure and magnetic behaviour of holmium-zirconium multilayers

2000 J. Phys.: Condens. Matter 12 3719

(http://iopscience.iop.org/0953-8984/12/15/318)

J. Phys.: Condens. Matter **12** (2000) 3719–3736. Printed in the UK PII: S0953-8984(00)06378-5

Structure and magnetic behaviour of holmium–zirconium multilayers

A Baudry†§, P Boyer†‖, M Brunel‡ and M C Luche†¶

† Departement de Recherche Fondamentale sur la Matière Condensée, CEA Grenoble, 17 rue des Martyrs, 38054 Grenoble Cédex 9, France

‡ Laboratoire de Cristallographie, CNRS, BP 166, 38042 Grenoble Cédex 9, France

Received 27 July 1999, in final form 3 March 2000

Abstract. Ho films of thickness varying from 100 Å up to 4000 Å and [Ho(x Å)–Zr(y Å)]$_n$ multilayers with $7 \leqslant x, y \leqslant 30$ were grown by evaporation under ultravacuum conditions on an oxidized Si(100) substrate covered with a Zr buffer layer. The x-ray diffraction patterns recorded for the transferred momentum $\vec{q}$ either along the $\vec{c}$-axis or in the basal plane of the hexagonal close-packed structure show that holmium suffers a permanent in-plane compression in films thinner than 200 Å and Ho(x Å)–Zr(30 Å) multilayers with $x \leqslant 30$. Low-temperature magnetization measurements indicate that the magnetic behaviour of Ho is strongly modified by epitaxial strains. The data are consistent with an enhancement of in-plane ferromagnetic order inside the Ho blocks in the Ho–Zr multilayers. A periodic dependence of the squareness of the hysteresis loop on the thickness of the Zr layers is observed in Ho(30 Å)–Zr(x Å) multilayers, which gives evidence for the existence of interlayer magnetic coupling. The out-of-plane magnetic anisotropy generated by Ho–Zr interfaces in a series of Ho(x Å)–Zr(30 Å) multilayers is found to be strong enough to compensate the in-plane anisotropy as the thickness of the Ho layers is decreased to about three monolayers. The variation of the anisotropy against the Ho layer thickness is satisfactorily reproduced with a rough crystal-field model using the point-charge approximation.

1. Introduction

Much attention has been paid in recent years to the magnetic properties of rare-earth (RE) thin films inserted in superlattices (SLs) where RE blocks comprising a few atomic layers are separated by thin non-magnetic metallic layers (NM) of, for example, Sc, Y, Zr or Lu. Some features have appeared as characteristic of the magnetism in such artificial nanoscaled periodic structures:

(i) The magnetic phase diagram is strongly modified, mainly as the result of strains induced by epitaxial growing conditions [1–7, 12]. In particular, the trend towards ferromagnetic ordering has been found to be either enhanced or suppressed according to whether the RE is subjected to either lateral compression (as in RE–Lu and RE–Zr SLs) or dilation (as in RE–Y SLs). Except in Tm–Zr multilayers [8], the enhancement of the trend towards ferromagnetic ordering as a result of finite-size effects in RE blocks comprising a finite number of atomic planes [9] does not seem to be decisive for determining the magnetic properties of these systems.

§ Affiliated to the CNRS.
‖ Affiliated to Université Joseph Fourier, Grenoble.
¶ Current address: Motorola Incorporated, France.

0953-8984/00/153719+18$30.00

(ii) In RE–Y and RE–Lu SLs where the lattice misfit is small (∼2%), coherent epitaxy is possible and the magnetic ordering in the RE layers propagates coherently across the non-magnetic layers, the coherence being maintained over many bilayers [1, 10]. The only effect of the non-magnetic spacer is to introduce a phase shift in the spin-density wave of the helimagnetic phase which takes place in the RE blocks below the Néel temperature. It is worth noting that the existence of a magnetic interlayer coupling across the non-magnetic spacer has been briefly mentioned for Ho–Zr multilayers which do not offer coherent epitaxial conditions owing to the large lattice misfit between Ho and Zr [11]. We go back to this point in more detail later on.

(iii) In RE–Zr SLs where coherent epitaxy does not exist owing to the rather large lattice misfits (∼10%), the contribution of the interfaces to the magnetic anisotropy increases as the thickness of the RE blocks decreases. In Dy–Zr SLs the interface anisotropy equilibrates the in-plane volume anisotropy when the thickness of the Dy blocks goes down below 10 Å [12]. However, such a compensation between the two contributions does not occur in Tm–Zr SLs where the magnetic anisotropy of Tm remains along the *c*-axis as in the bulk [8].

Quite recently, a series of papers have reported on the structure and magnetic properties of Ho–Y [6, 13] and Ho–Lu [7, 14] superlattices. These works were motivated by the interest in comparing the magnetic structure of Ho as observed in such superlattices to that of bulk Ho. Ho has the peculiarity of displaying a quite rich variety of magnetic phases according to the value of the temperature and applied magnetic field [15], and that makes it a good candidate for helping us to understand why the magnetic phase diagrams of RE in RE–NM superlattices strongly differ from the measured ones for the bulk. The main results which stand out from such studies can be summarized as follows:

(i) In Ho–Y SLs, the neutron scattering data are consistent with the assumption that there are helical spin waves in both the Ho and Y blocks, with different turn angles in the Ho and the Y. However, the Néel temperature and the low-temperature turn angle are reduced as compared to the bulk values [6]. The reduction of the ordering temperature of the Ho moments and the suppression of the low-temperature cone phase have found confirmation in the results of further magnetization measurements [13]. These effects are attributed to the strain imposed by the epitaxial growth process, which reduces the maximum in the indirect exchange coupling. Moreover, the *c*-axis cone phase present in bulk Ho below 20 K is suppressed. The existence of high-order magnetic satellites in the neutron diffraction spectra indicates that the moments are instead bunched around the six easy axes in the basal plane and form long-period, commensurate spin-slip structures.

(ii) In Ho–Lu SLs, the zero-field neutron diffraction experiments reveal the existence of a ferromagnetic transition at low temperature in strained samples [7]. The ferromagnetic phase is stabilized by applying a magnetic field in the basal plane. As in the bulk, a fan structure intermediate between the helical and ferromagnetic states is found; however, the critical field required to drive the sample ferromagnetic is significantly lowered. Magnetization measurements have shown that a ferromagnetic phase arises at low temperatures instead of a cone phase. The in-field transition to ferromagnetic order occurs at lower fields than in the bulk, and there is no clear evidence for the existence of intermediate fan structures. These results are qualitatively interpreted as indicative of a stabilization of the ferromagnetic state by the in-plane compressive strain resulting from the Ho/Lu lattice mismatch. This interpretation has been confirmed by the results of magnetoelastic stress measurements conducted under a magnetic field on Ho–Lu (and Ho–Y) SLs [14, 16].

In the present paper we present the results of magnetization measurements performed on Ho–Zr multilayers. This work is part of a more extensive investigation of the magnetism in RE–Zr multilayers. Our interest in such systems lies in the large difference between the hcp lattice constants of the two metals and the very small miscibility of Zr with RE elements below 500 °C. The large lattice misfit between Zr and RE metals prevents a fully coherent epitaxial growth, but allows one to expect significant strain effects on the magnetism of the rare earth. At the same time, abrupt interfaces without interdiffusion are expected in these periodic structures. Interface profiles extending over at most three atomic distances were actually observed in Dy–Zr multilayers by high-resolution electron microscopy [12]. The nature of the interfaces is a determinant for the behaviour of the magnetic anisotropy, and the absence of chemical intermixing is propitious as regards using the results of simple crystal-field calculations for an instructive comparison with the experimental data. Let us mention that some of the data reported here are extracted from an unpublished PhD dissertation by M C Luche [17]. In addition, we shall refer later on to the results of magnetization and magnetoresistance measurements performed in high pulsed magnetic fields which have been the object of a brief report in a conference proceedings [11].

2. Sample preparation and characterization

Ho films with a thickness varying from 100 Å up to 4000 Å were deposited in an ultrahigh-vacuum chamber ($P < 10^{-7}$ Pa) using an effusion cell, on a (100)-oriented Si substrate oxidized over ∼40 Å and previously covered with a 200 Å Zr buffer layer. The temperature of the substrate was maintained at ∼300 °C during the deposition achieved at a rate of ∼0.5 Å s^{-1}. The films were protected from oxidization by a 100 Å Cu capping layer. A series of [Ho(x Å)–Zr(y Å)]$_{25}$ multilayers (denoted as Hox–Zry hereafter) were grown in similar conditions on a Si substrate covered with a 600 Å buffer layer of Zr. Zr was electron-beam evaporated at a rate of ∼1 Å s^{-1}. The residual pressure of various elements was measured during the deposition using a quadrupole analyser. Typically, the oxygen and hydrogen pressures were maintained below 10^{-9} Pa and 10^{-7} Pa respectively. The deposition rates and layer thicknesses were monitored with a quartz oscillator. The nominal chemical period was found to be smaller than the period deduced from careful analysis of x-ray diffraction spectra recorded at both small and large Bragg angles by at most 15% for all the samples investigated, the deviation being larger for multilayers incorporating Zr layers thinner than 20 Å.

The θ–2θ x-ray diffraction patterns recorded in the reflection geometry for the Ho films deposited on a 200 Å Zr layer (Zr–Ho bilayers) show narrow lines of strong intensity corresponding to the (002) Bragg reflections of Ho and Zr and a very small contribution of the (100) and (101) reflections. This is indicative that the Ho films display a strong texture along the (002) direction. From the width of the (002) line the coherence along the growth direction was estimated to be about 300 Å in 4000 Å and 900 Å films. It is worth noting that the position observed for the (002) Bragg line of Ho in the 100 Å film corresponds to an interplane spacing of 2.7831 Å, which represents a relative *compressive* strain of ∼−0.85% along the c-axis direction in comparison with the bulk value (2.806 Å). At the same time, no significant change in the interplane spacing is found for the underlying Zr layer with respect to that measured in the bulk (2.5735 Å).

Typical x-ray θ–2θ scans performed on Hox–Zry multilayers around the (002) Bragg reflections of Ho and Zr are shown in figure 1. Five satellites are clearly distinguished for all the samples comprising Ho blocks thicker than 10 Å, which is characteristic of a well-defined periodic structure with rather sharp interfaces. Rocking curves recorded for a fixed θ-value show that the dispersion of the growth orientation around the (002) direction varies between

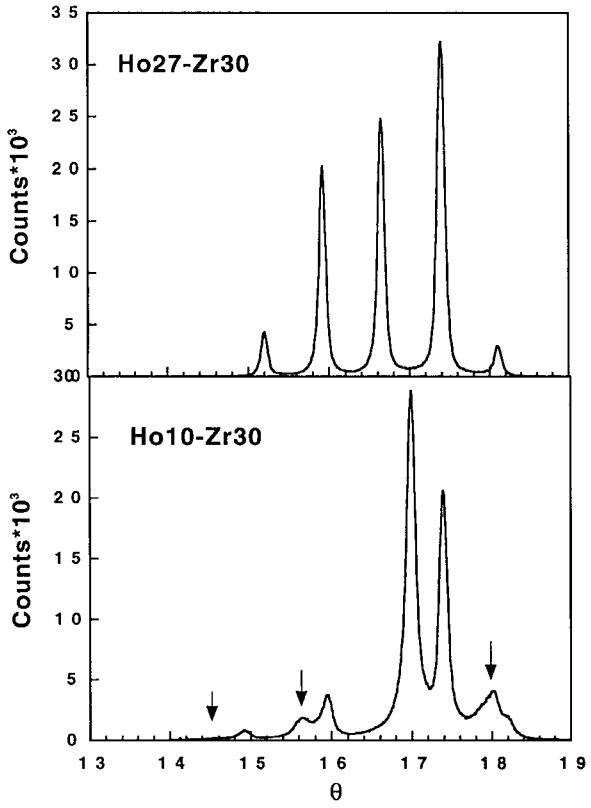

Figure 1. X-ray θ–2θ diffraction spectra measured for two [Hox–Zr]$_{25}$ multilayers around the (0002) Bragg reflections. The lower spectrum indicates the coexistence of two growth directions along the (0002) and $(10\bar{1}1)$ axes of the close-packed hexagonal structure. The lines which correspond to the $(10\bar{1}1)$-oriented texture are identified by arrows. In each spectrum, the Bragg line close to $\theta = 17.5^\circ$ includes a strong contribution from the 200 Å Zr buffer layer.

3° and 4.5° in the various samples investigated. The linewidth measured for the stronger lines for several [Hox–Zr30]$_{25}$ multilayers is found to vary between 0.1° and 0.15°, which corresponds to coherence lengths which extend over eight to ten bilayers along the growth direction. Both the intensity and shape of the diffraction lines are quite well reproduced by using the model proposed by Locquet *et al* [18]. This model includes the imperfections localized at the interfaces in the calculation of diffracted intensities, assuming that the interfacial disorder is well represented by a Gaussian distribution of the interplane spacings. The correlation observed between the width of the distribution and the peak intensities and linewidths within a diffraction pattern is an indication that the interfacial disorder is responsible for the reduction in long-range order observed for many multilayers. For the Ho–Zr multilayers investigated, the comparison of the results given by the model with the diffraction data shows that the interfacial disorder is not very sensitive to the thickness of the Ho blocks, but increases significantly when the thickness of the Zr blocks is increased from 7 to 30 Å. This result suggests that interfacial disorder is mainly generated by imperfections such as rugosity or misorientation in the Zr layers.

As can be seen in figure 1, the Bragg pattern recorded for the Ho10–Zr30 multilayer presents a more complex structure which reflects the coexistence of two growth directions

along the (002) and (101) crystallographic axes respectively. The presence of the Zr(101) Bragg peak with a rather strong intensity in the x-ray diffraction patterns recorded under grazing incidence for several Ho–Zr bilayers and multilayers (see below) gives evidence that grains oriented away from the (002) direction exist in the Zr buffer layer. Such a misorientation in the buffer is very probably responsible for the emergence of the second growth direction observed in the multilayers including Ho blocks as thin as 10 Å or less. Notice that the same effect occurs in Dy–Zr SLs [17].

In-plane θ–2θ x-ray diffraction experiments were performed under grazing incidence (0.5°) on several Ho films and in Hox–Zry multilayers. Examples of grazing-incidence diffraction patterns are shown in figure 2. From the detailed analysis of the recorded spectra the following results can be pointed out (see tables 1 and 2):

Table 1. Variation of interplanar distances in Zr(200 Å)–Ho bilayers as measured from the grazing-incidence x-ray diffraction data. The reported values are relative to the distances measured in bulk metals.

Nominal composition	$\Delta d(100)/d(100)$, Zr	$\Delta d(100)/d(100)$, Ho
Zr200–Ho900	Reflection not observed	$\sim -0.1\%$
Zr200–Ho400	0.0%	$\sim -0.3\%$
Zr200–Ho100	0.0%	$\sim -0.8\%$

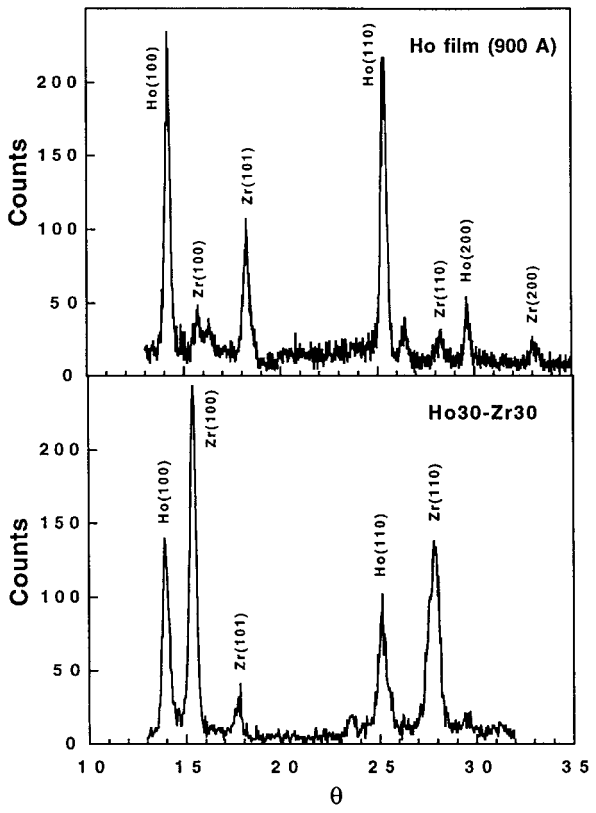

Figure 2. X-ray diffraction patterns measured under grazing incidence (0.5°) for a Ho film and a $[\text{Ho30–Zr30}]_{25}$ multilayer, deposited on a 200 Å Zr buffer layer.

Table 2. Variation of interplanar distances in Ho–Zr multilayers as measured from the grazing-incidence x-ray diffraction data. The reported values are relative to the distances measured in bulk metals.

Nominal composition	$\Delta d(100)/d(100)$, Zr	$\Delta d(100)/d(100)$, Ho
Ho30–Zr30	$\sim+0.3\%$	$\sim-0.8\%$
Ho20–Zr30	$\sim+0.4\%$	$\sim-2.4\%$
Ho12–Zr30	$\sim+0.0\%$	$\sim-2.0\%$
Ho30–Zr12	$\sim+0.8\%$	$\sim-1.6\%$

(i) No change in the position of the (100) Bragg reflection is observed for Zr in the bilayers. On the other hand, this Bragg line tends to move towards larger angles for Ho. Relatively to the bulk, no measurable shift is observed in the 4000 Å film. The shift is still small (0.2% and 0.3% respectively) in the 900 Å and 400 Å Ho films, but as large as 1.8% in the (100 Å) Ho film which is therefore subjected to an in-plane relative compression of $\sim-0.8\%$. The amplitude of the in-plane compression is close to that measured along the $\vec{c}$-direction (see above). Similar results are obtained from the (110) reflection, with a smaller amplitude however, which is an indication that the in-plane strain may be not isotropic. As mentioned above, the (101) reflection of Zr appears in all the recorded spectra, which reflects some misorientation in the 200 Å Zr underlayer with respect to the (002) direction (only $(hk0)$ reflections should appear for a (002)-oriented layer).

(ii) The Bragg patterns recorded for Hox–Zr30 multilayers display an increasing shift of the (100) reflection of Ho as the thickness of the Ho layers decreases. The shift corresponds to an in-plane compression of -0.8% in the Ho30–Zr30 multilayer and of -2.0% in the Ho12–Zr30 multilayer. No significant shift is observed for the (100) line of Zr. These results indicate that the relaxation is not completed for the 30 Å Ho layers in which a rather strong lateral compression remains. The same effect was previously observed for Dy30–Zr30 multilayers [12].

(iii) The in-plane diffraction pattern recorded for a Ho30–Zr12 multilayer reveals that Zr is expanded by +0.8% and Ho is compressed by -1.6%. These values are consistent with the in-plane relative compression measured for Ho in the Ho30–Zr30 multilayer.

In conclusion, the holmium suffers a permanent in-plane compression in films thinner than 200 Å as deposited on a 200 Å Zr underlayer and in the Ho–Zr superlattices. A very similar situation was reported for Dy–Zr multilayers in which an interfacial coherence corresponding to a partial lattice relaxation with creation of misfit dislocations was revealed by high-resolution electron microscopy [12]. Qualitatively the results are roughly understood on the basis of the simple model developed by Bruno and Renard [19]. From this model, taking into account the mismatch of $\sim$10% between the lattice parameters of Ho and Zr, the critical thickness t_c below which pseudomorphic epitaxy takes place is estimated at $\sim$10 Å (4 ML) for a holmium film grown on a 200 Å zirconium buffer layer. It is reduced to $\sim$2.5 Å, i.e. 1 ML, for the Hox–Zr30 multilayers.

3. Magnetization measurements

The results of magnetization measurements performed in the temperature range 8 K–300 K using a SQUID magnetometer for several *field-cooled* Ho films with a constant in-plane applied field of 500 Oe are displayed in figure 3. In the 4000 Å Ho film, the paramagnetic–antiferromagnetic transition is clearly observed at $T_N = 130$ K. Above the Néel temperature, the magnetization obeys a Curie–Weiss law characterized by $\theta = 87.0 \pm 0.4$ K and a magnetic

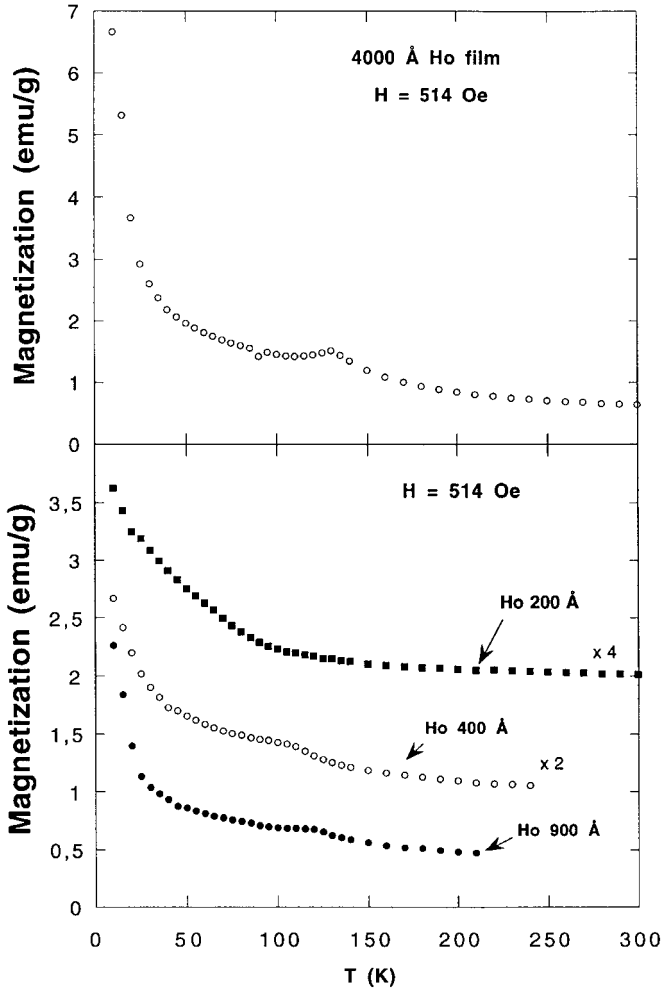

Figure 3. The temperature dependence of the magnetization in field-cooled Ho films deposited on a 200 Å Zr buffer layer. The curves in the lower part of the figure correspond to 900 Å (dots), 400 Å (open circles) and 100 Å (squares) Ho films respectively.

moment $\mu = 11.2\ \mu_B$. These values are very close to those observed for Ho bulk (88 K and 11.2 μ_B respectively [15]). From ~35 K downwards, the magnetization is readily increasing which corresponds to *in-plane* ferromagnetic ordering. A fairly similar behaviour is observed for the 900 Å Ho film; however, the Néel temperature is lowered to 116 K. In the 400 Å Ho film, the antiferromagnetic transition can still be observed at 112 K together with a fast increase of the magnetization below 50 K. The transition is no longer clearly visible in either the 200 Å or the 100 Å Ho film. In contrast to the case for the thicker films, the magnetization for these two films is steadily increasing from $T \sim 100$ K down to 10 K, the slope becoming steeper below 20 K. This behaviour suggests that the transition from the paramagnetic state to ferromagnetic order is spreading out over several tens of degrees below 100 K. The reduction of T_N as the thickness of the Ho film decreases, and the suppression of the antiferromagnetic phase in the Ho films for a thickness $t_{\mathrm{Ho}} \leqslant 200$ Å are very probably the result of residual

strains induced by the epitaxial growth of holmium on zirconium. Remembering the above-mentioned compression ($\sim -0.8\%$) of the Ho lattice observed in the H100–Zr200 bilayer, and using the value of $\sim$70 GPa for the Young modulus in bulk holmium [20], a rough estimation of the stress $\sigma_a = E\epsilon_a$ with $\epsilon_a = 0.8\%$ leads to $\sigma_a \approx 0.55$ GPa. No data are available to our knowledge concerning the magnetic behaviour of holmium under high pressures. It is not unreasonable however to expect this behaviour to be not too different from that observed for dysprosium. In this rare earth, from the data reported by Bartholin *et al* [21], a shift of $\sim$70 K toward the high temperatures is anticipated for the antiferromagnetic–ferromagnetic transition under a pressure of $\sim$6 kbar (0.6 GPa). Shifts of this order of magnitude were actually observed for T_C in Dy-based multilayers where the Dy layers are compressed by epitaxy [12]. Referring to the results relating to Dy and Dy-based superlattices, it appears quite plausible that in-plane ferromagnetic order set in at $\sim$100 K, i.e. a temperature about 80 K higher than for the holmium bulk, in constrained holmium films such as the 100 Å and 200 Å films studied here. This enhancement of the trend towards ferromagnetic ordering is reasonably attributed to compression which results in a change in the magnetoelastic energy of the magnetic film (it has been recognized for a long time that the magnetoelastic energy decisively controls magnetic ordering in rare-earth metals [22]). On the other hand, the large spreading out of the ferromagnetic transition as observed in these samples is most probably related to the imperfections displayed by the microstructure of the holmium film such as grain boundaries and/or possible variations of the film thickness, which are able to generate strain inhomogeneities.

An illustration of the *zero-field-cooled–field-cooled* magnetization curves measured for the Ho–Zr multilayers is shown in figure 4. No sign of the existence of an antiferromagnetic phase can be clearly distinguished. On the other hand, these curves display a large thermal irreversibility with a varied behaviour depending on the thickness of the Ho blocks. For instance, the behaviour observed in the Ho30–Zr30 multilayer is typical of an assembly of antiferromagnetically coupled grains with a blocking temperature $T_B \sim 100$ K fairly close to the Néel temperature and a freezing temperature $T_G \sim 25$ K of the magnetization along the random directions of anisotropy. On the other hand, the magnetization curve observed for the Ho12–Zr30 multilayer is rather typical of an assembly of ferromagnetically coupled grains ($T_B \sim 60$ K). Moreover, the structure corresponding to successive 'plateaux' as observed in the magnetization curve below 80 K could result from a lack of homogeneity in the thickness of the holmium blocks. In figure 4 we have also reported the zero-field-cooled–field-cooled magnetization pattern recorded for the 900 Å Ho film, which does not display any thermal hysteresis. These results show that the magnetism of Ho is significantly perturbed by the proximity of Zr layers. Magnetization *isotherms* $M(H)$ were measured for several samples at various temperatures, varying the in-plane applied field between 0 and 5.5 T. For the 900 Å Ho film the magnetization curve measured at 10 K with the applied field in the plane of the film displays a small plateau between 0.2 T and 0.4 T corresponding to a magnetization of about 40 emu g^{-1}, followed by a rather fast increase up to a value of 288 emu g^{-1} at 5.5 T (see figure 5). The finite slope of the $M(H)$ curve at high fields indicates that the saturation is not reached. The value of the magnetization at 5.5 T is close to that measured in the bulk for an applied field along the $\vec{a}$-axis and lower than the value $\sim$340 emu g^{-1} measured with the field along the $\vec{b}$-direction [23]. The critical field associated with the helical antiferromagnetic–ferromagnetic transition and defined by the change in the curvature of the $M(H)$ plot is about 0.9 T, i.e. much higher than the value found in bulk Ho ($\sim$0.2 T). These results are consistent with the existence of strong pinning of the orientation of magnetic moments at grain boundaries inside the in-plane disoriented granular microstructure of the film. Figure 5 also displays the $M(H)$ curve measured with the applied field perpendicular to the film plane. This curve corresponds well

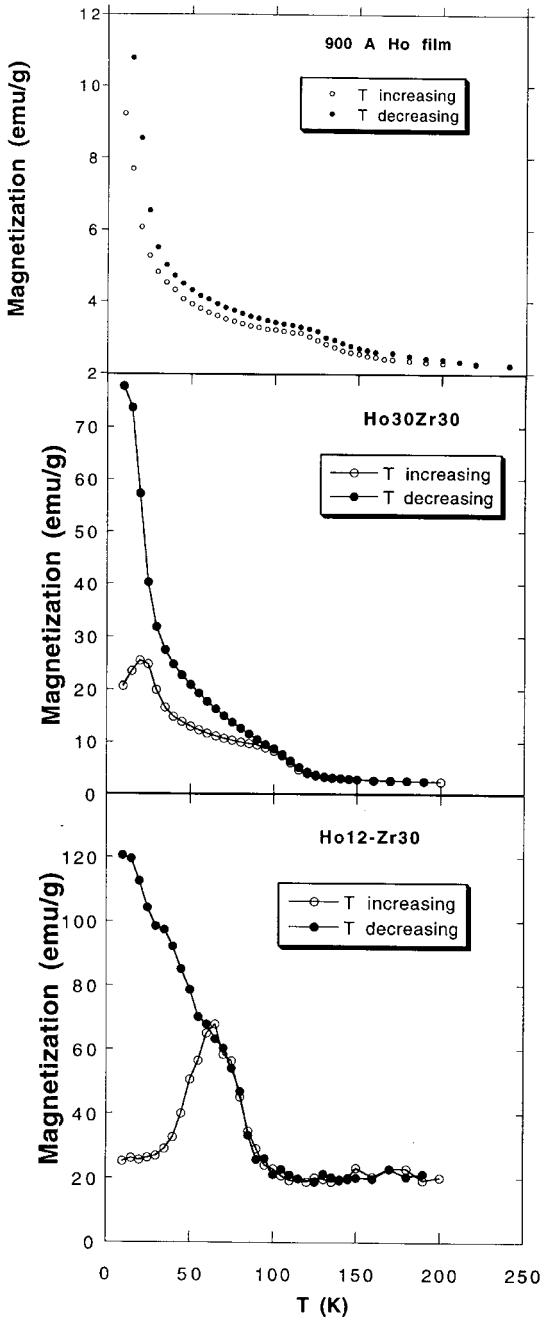

Figure 4. Zero-field-cooled–field-cooled ($H = 514$ Oe) magnetization curves measured for a 900 Å Ho film and two $[Hox–Zr30]_{25}$ multilayers.

to the behaviour observed in the bulk for a magnetic field along the magnetically hard $\vec{c}$-axis. For this magnetic field configuration, the magnetization reaches the value $\sim$70 emu g^{-1} at 5.5 T and no saturation is observed.

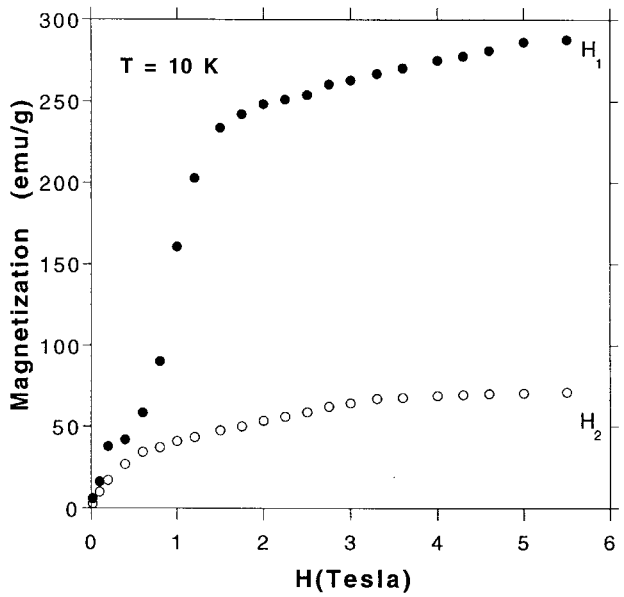

Figure 5. Magnetization isotherms measured for the 900 Å Ho film with the applied magnetic field either parallel (H_1) or perpendicular (H_2) to the film.

The $M(H)$ data recorded for the [Ho30–Zr30]$_{25}$ multilayer at various temperatures in the range 10–130 K are plotted in figure 6. The magnetization measured at 10 K with an in-plane applied magnetic field of 5.5 T is about 300 emu g^{-1}. This value is both very close to the value obtained for the 900 Å Ho film and rather far from saturation. Experiments performed at 77 K in pulsed high magnetic fields indicate that saturation is actually reached around 20 T

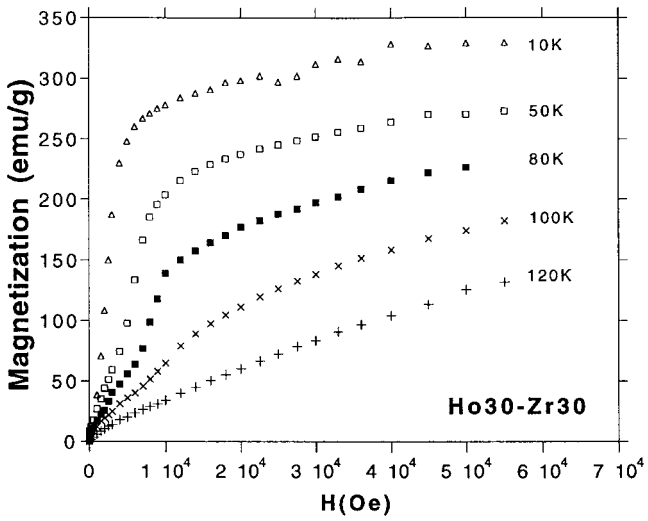

Figure 6. Magnetization isotherms measured for a [Hox–Zr30]$_{25}$ multilayer with the applied magnetic field in the plane of the film.

[24]. The point of major interest in the curves is the variation of the critical field H_c with temperature. H_c is steadily increasing with temperature up to a maximum value ∼0.9 T at 100 K, then drops to ∼0.1 T at 120 K and cancels at 130 K. The H_c–T plot is shown in figure 7. In the same figure we have included for comparison the data taken from Féron [25] for monocrystalline Ho and those from Tomka *et al* [14] for a Ho–Lu superlattice. These data clearly show that the critical field is strongly reduced in the two superlattices in which the Ho lattice suffers a lateral compression induced by the epitaxial growth conditions. The observed effect in the Ho–Zr superlattices is in full agreement with the conclusion reached by Tomka *et al* [14] that the trend towards ferromagnetism is stabilized by the lattice mismatch strain in the Ho–Lu superlattice. This trend can be further enhanced by finite-size effects which favour ferromagnetic alignment of the outermost spins in the spin-slip magnetic structure of the Ho slabs as demonstrated by mean-field calculations [9].

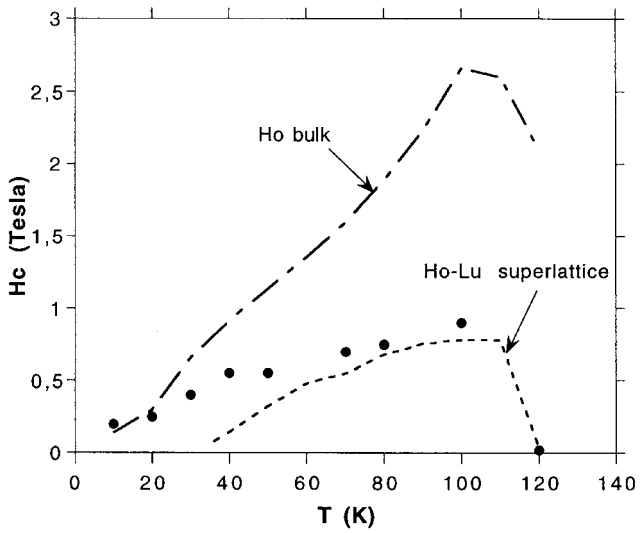

Figure 7. The temperature dependence of the critical field in the Ho–Zr multilayers (dots). The figure allows a comparison of the data with the results reported by Féron [25] for monocrystalline Ho and by Tomka *et al* [14] for a Ho–Lu superlattice.

Examples of hysteresis loops recorded at 10 K for Hox–Zr30 multilayers are shown in figure 8. For the [Ho27–Zr30]$_{25}$ multilayer the diagram obtained with an in-plane applied magnetic field is characteristic of a ferromagnetic material. The remanent magnetization is ∼80% of the saturation value and the coercive field is ∼0.25 T. Such values are indicative of a rather easy in-plane ordering of the ferromagnetic domains inside the Ho layers, contrary to the situation for Dy–Zr multilayers of similar composition where much larger coercive fields (∼1.2 T) and smaller remanence show the existence of pinning of the ferromagnetic domains by strong local anisotropy fields in the Dy layers [12]. As the thickness of the Ho blocks decreases from 30 Å down to 12 Å, the hysteresis loop broadens and simultaneously shows a slower and slower approach to saturation, a decreasing remanent magnetization and an increasing coercive field up to 0.35 T. The increasing coercivity can be understood as the result of a growing contribution of interfaces in pinning the magnetic moments. For the samples comprising Ho blocks thinner than 12 Å, the hysteresis loop appears as both stretched and narrowed, which indicates an increasing hardness for in-plane magnetic ordering. The remanent magnetization turns out to be quite small (only 10% of the magnetization at 5.5 T

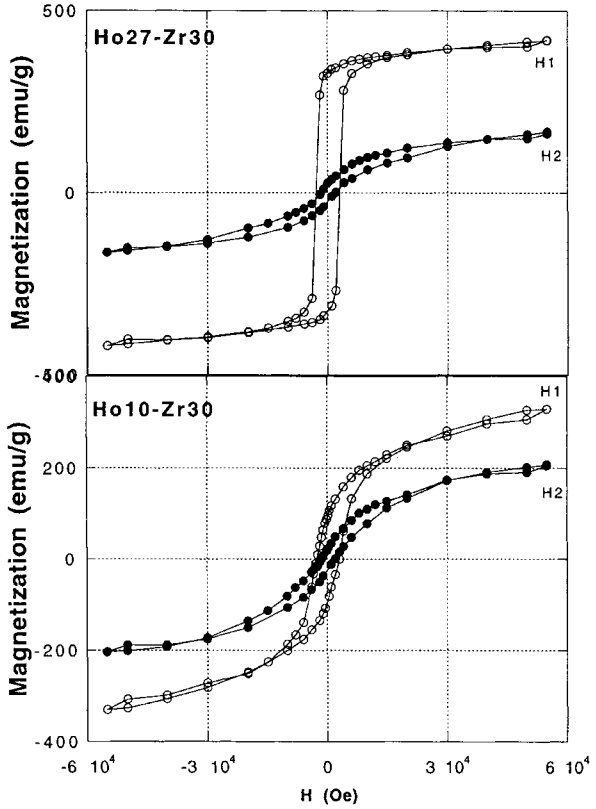

Figure 8. Hysteresis loops measured at 10 K for two $[Ho–Zr]_{25}$ multilayers with the applied magnetic field either parallel (H_1) or perpendicular (H_2) to the plane of the layers.

in the Ho7–Zr30 multilayer) and the coercivity is decreasing from 0.35 T for the Ho12–Zr30 sample down to 0.16 T for the Ho7–Zr30 sample.

Hysteresis loops were also recorded for several multilayers, varying the thickness of the Zr blocks from 7 to 30 Å whereas the thickness of the Ho blocks was kept fixed at 30 Å. The shape of the loop is well characterized by the squareness $S = M_r/M_{s0}$, where M_r is the remanent magnetization and M_{s0} the magnetization obtained by zero-field extrapolation of the line of approach to saturation. As can be seen in figure 9, S roughly varies periodically with the thickness of the Zr blocks. The oscillations have a period of approximately 15 Å, i.e. about six Zr monolayers, and an amplitude corresponding to a relative variation of about 25%. Such an oscillatory dependence of the squareness on the thickness of the spacer between the magnetic blocks was observed for the first time for Gd–Y superlattices [26] and is considered a signature of magnetic interlayer coupling.

The interlayer coupling in RE–Y superlattices is reasonably well understood on the basis of an oscillating RKKY-type interaction [27]. In its rough version the model is based on the calculation of the long-range RKKY interaction between RE interfacial planes embedded in bulk yttrium, neglecting the strains imposed by epitaxial conditions and relying on the close similarity between the band structures of RE metals and Y. Atoms inside a RE layer are assumed to be coupled via the usual exchange interaction as in the bulk metal. When applied to Gd–Y superlattices the model leads to a periodically oscillating exchange-coupling

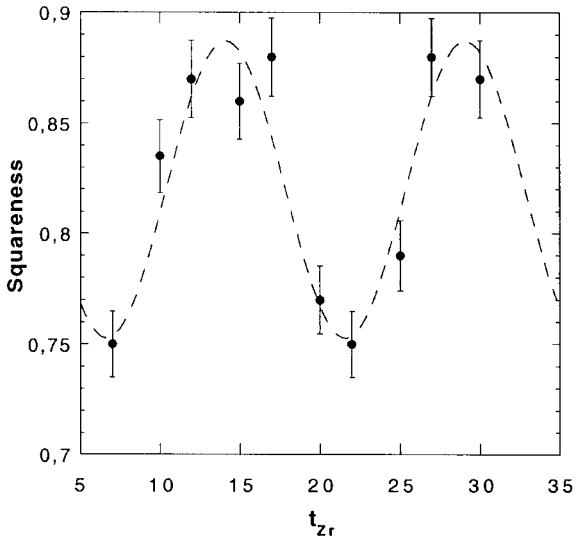

Figure 9. Variation of the squareness S of the hysteresis loop against the thickness of the Zr blocks in the [Ho30–Zrx]$_{25}$ multilayers. The dashed line corresponds to the function $\sin([2\pi/\Lambda]x)$ fitted to the data, where x is the thickness of the Zr layer assumed to vary continuously.

function $J(n)_{\mathrm{Gd-Y}}$ for coupling between Gd planes separated by n planes of Y. The periodicity corresponds to $n \approx 7$, in good agreement with the experimental observations. As a result, the arrangement of the magnetic moments of the Gd layers within the superlattice oscillates between ferromagnetic and antiferromagnetic alignment with the same periodicity. It should be pointed out that the oscillating behaviour of the function $J(n)_{\mathrm{Gd-Y}}$ is critically determined by the dependence of the susceptibility $\chi(q)$ of Y on the wave-vector component q along the c-axis of the hcp structure. The function $\chi(q)$ itself is controlled by the topology of the Fermi surface of the non-magnetic metal.

More generally, it was recently argued that the RKKY model is able to explain the large periods observed in many nanostructured systems for the oscillatory coupling between ferromagnetic layers separated by a non-magnetic metal, provided that the discrete variation of the spacer thickness is taken into account [28–30]. The period of the oscillations anticipated by the simple RKKY model applied to a continuous medium is $\Lambda = \pi/k_f \sim 1$ ML, i.e. $\sim$2.5 Å for Zr. It is seen that the six-times-larger apparent period actually observed in the Ho–Zr superlattices can be easily explained by the Vernier effect which results from the discrete sampling of the fast RKKY oscillation by a finite number of Zr planes. The reduced amplitude of the oscillations is attributed to the existence of interfacial defects and roughness generated by the large difference between the basal-plane lattice constants of Zr and Ho. Actually, it can be shown that interfacial disorder gives rise to incoherent scattering of the conduction electrons and then results in blurring of the interlayer coupling oscillations [29]. This is the reason invoked to explain why only short-range magnetic coherence extending over only 2–3 bilayers is observed in Ho–Sc superlattices [31] in contrast to the long-range coherence displayed by Ho–Y superlattices, although Sc and Y have quite similar Fermi surfaces. In the Ho–Sc system the large difference ($\sim$7%) between the basal-plane lattice constants of the two metals generates a large number of structural defects. On the other hand, the lattice mismatch is only $\sim$2% in the Ho–Y system and allows one to grow epitaxial structures with a high degree of crystallographic perfection. Ho–Zr superlattices are clearly expected to display structural

properties rather similar to those of the Ho–Sc system, and the coherence length of magnetic coupling probably does not exceed a few bilayers. Blurring of the coupling oscillations can be also qualitatively understood within the Vernier picture by considering that the number of separating Zr planes between successive Ho layers fluctuates because of interface roughness.

Finally, let us mention as additional support for the notion of the existence of magnetic interactions between Ho blocks the oscillation of magnetoresistance measured under high magnetic field (5 T) in the same set of Ho30–Zrx multilayers [11]. It is of interest also to see that no significant oscillations characteristic of RE interlayer coupling was observed in other RE–Zr systems such as Dy–Zr [12] or Tm–Zr [8] multilayers.

4. Magnetic anisotropy

Magnetization isotherms were recorded at 10 K for a set of Hox–Zr30 multilayers, with the applied magnetic field either parallel or perpendicular to the film plane. Some of them are plotted in figure 10. These plots clearly demonstrate the growing contribution of interfaces to creating an out-of-plane magnetization which tends to balance the in-plane volume magnetization as the thickness of the Ho blocks is reduced below ∼10 Å.

Magnetic anisotropy in nanosized Ho films is almost exclusively determined by the magnetocrystalline anisotropy which dominates over the magnetostatic contribution by about two orders of magnitude. The anisotropy energy can be therefore expressed to a very good approximation as

$$K = K_v + 2K_s/t \tag{1}$$

where t is the thickness of the Ho slab, and K_v and K_s are the volume and interface anisotropy constants respectively. Figure 11 shows the variation of the product Kt against t for the Hox–Zr30 multilayers investigated. The anisotropy K was estimated by extrapolating the magnetization curves toward the saturation using the following expression:

$$M(H) = M_s\left[1 - \sum_n \frac{a_n}{H^n}\right] \tag{2}$$

where M_s is the magnetization at saturation and n an integer. The summation was in practice limited to $n = 4$. This procedure led to values of saturation fields around 20 T in reasonable agreement with the results of magnetization measurements performed under high pulsed magnetic fields on a $[\text{Ho30–Zr30}]_{160}$ sample [24]. Moreover, the magnetic anisotropy estimated in this way for the 900 Å Ho film is $\sim -4 \times 10^8$ erg cm^{-3}, i.e. ∼70 K/atom. This value is of the right order of magnitude as compared to the values reported for bulk Ho [32]. Although an accurate determination of the magnetic energy is impossible owing to the very high values of the saturation fields, we are confident that our procedure provides a reasonable estimate of the magnetic anisotropy.

In deducing equation (1) the layers are considered as continuous media and the thickness of interfaces is neglected. If such rough assumptions are removed and the discreteness of the Ho layers is taken into account, a more realistic expression for the product Kt_{Ho} of the *effective* anisotropy in terms of the thickness of the Ho slabs in a Hox–Zr30 multilayer is [12]

$$Kt_{\text{Ho}} = (t_{\text{Ho}} - n_s d)K_v + n_s K_s \tag{3}$$

where n_s is the number of interface planes and d the lattice spacing in the growth direction. Referring to the high-resolution electron microscopy results relative to the interface profiles in Dy–Zr superlattices [12], it appears that taking $n_s = 2$ is a reasonable assumption, in agreement

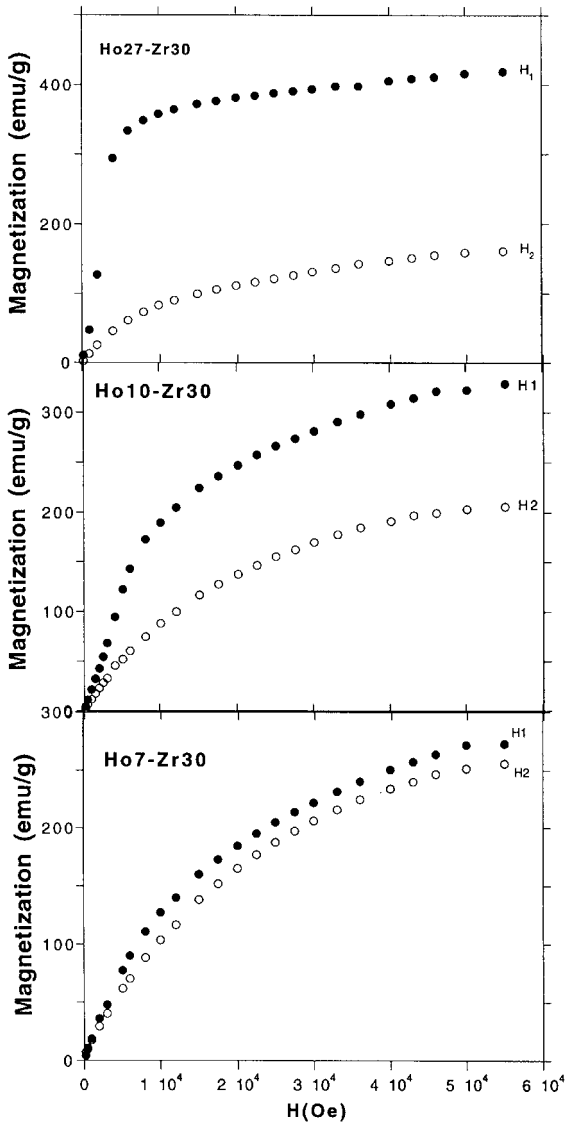

Figure 10. Magnetization isotherms ($T = 10$ K) measured for several [Hox–Zr30]$_{25}$ multilayers with the applied magnetic field either parallel (H_1) or perpendicular (H_2) to the plane of the layers.

with the quite low miscibility between Zr and RE metals. For $K = 0$, the following relation then holds:

$$\frac{K_s}{K_v} = d - \frac{t_{c\mathrm{Ho}}}{2} \tag{4}$$

where $t_{c\mathrm{Ho}}$ is the thickness of Ho slabs for which the interface and volume anisotropies compensate each other. Clearly equations (3) and (4) are meaningless if $t_{\mathrm{Ho}} < 3d$.

Qualitatively, it can be deduced from the data reported in figure 11 that the thickness $t_{c\mathrm{Ho}}$ at which the compensation occurs is about 8 Å, i.e. three Ho monolayers. On the other hand, the variation of the product $K t_{\mathrm{Ho}}$ with t_{Ho} roughly obeys a linear law determined by the

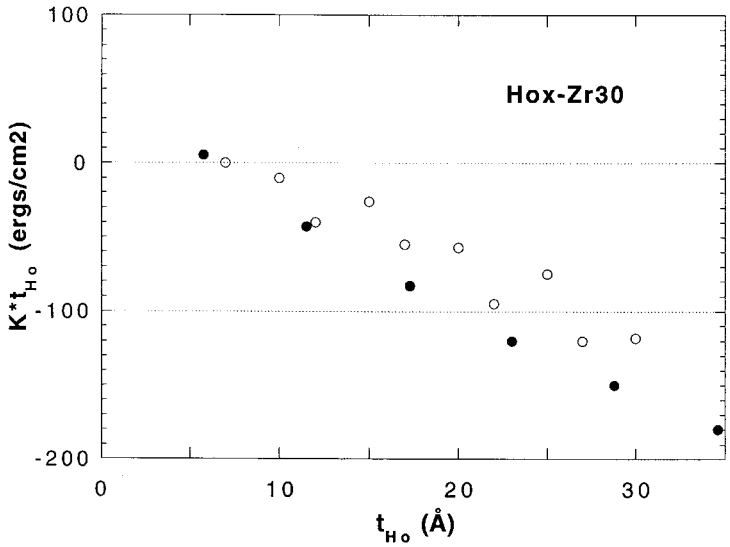

Figure 11. A plot of the product Kt_{Ho} against the thickness of the Ho layers for the [Hox–Zr30]$_{25}$ multilayers (open circles). K is the anisotropy deduced from the magnetization curves using the procedure described in the text. The error on the experimental values is estimated at ∼10%. The results of crystal-field calculations (spots) are given for comparison.

values $K_v \sim -5 \times 10^8$ erg cm^{-3}, $K_s \sim 20$ erg cm^{-2} for the volume and interface anisotropy coefficients respectively. Referring to the results previously reported for Dy–Zr multilayers [12], it is seen that both t_c and K_s are very close in the two systems.

Calculations of the magnetocrystalline anisotropy were performed within the point-charge approximation limited to the fourth-order terms, following the procedure indicated in a previous paper [12]. As indicated in reference [12], non-zero values of the fourth-order crystal-field parameters can result from slight distortions from the hexagonal symmetry, generated by incoherent epitaxial growth.

The results of such calculations performed with effective charges $q_{\mathrm{Ho}} = 0.3e$, $q_{\mathrm{Zr}} = 0.4e$ on the metal-ion sites are plotted in figure 11. The ratio of ion charges was taken equal to 3/4, in agreement with the effective charges deduced from electric field gradient measurements on Zr and Gd metals [33]. On the other hand, the values of the net electric charges assigned to Zr and Ho atoms in order to reproduce the experimental anisotropies may appear surprisingly small. However, it is well known that no clear physical meaning can be given to the absolute values of effective point charges in relation to the crystal field [34]; they should rather be considered as fitting parameters. Several calculations were performed assuming different atomic configurations in the Ho–Zr interface planes, corresponding to either incoherent or partially coherent epitaxy. The in-plane compression observed for the Ho layer was also taken into account. As previously mentioned for Dy–Zr multilayers [12], the results provided by the point-charge model are actually very little dependent on the structure of the Ho–Zr interfaces. It can be seen from figure 11 that the calculated values of the anisotropy fit the experimental data reasonably well. However, it is worth noting that the quantity Kt_{Ho} as calculated within the point-charge approximation deviates to some extent from the linear behaviour against the thickness of the Ho blocks: the variation rate decreases as the thickness of Ho layers increases, and becomes constant for $t_{\mathrm{Ho}} > 50$ Å as might reasonably be expected for thick Ho layers in which the magnetic anisotropy is entirely dominated by the volume contribution. The

asymptotic slope of the curve then corresponds to the value of K_v. Such a non-linear behaviour of the product $K t_{\mathrm{Ho}}$ is indicative that the model assuming an interface anisotropy described by a surface term k_s is oversimplified. A better picture should incorporate some distribution of the interface contribution spreading out over several atomic planes inside the Ho layer.

5. Summary

From the study reported in this paper several interesting points emerge concerning the magnetism of Ho in thin films and Ho–Zr multilayers incorporating Ho blocks 30 Å thick or less. First, the strong influence of lateral compression induced by epitaxial conditions on the magnetic properties of the Ho layers, as previously observed by the Oxford Group in Ho–Lu superlattices [14], is clearly confirmed. As the main effect of epitaxial strain, the trend towards ferromagnetic order is strongly enhanced. In Ho films deposited on a 200 Å Zr buffer layer, the Néel temperature corresponding to the paramagnetic–helical antiferromagnetic transition decreases with the thickness of the film from the bulk value $T_N = 130$ K down to about 100 K, the transition being hardly distinguished in films thinner than 200 Å which suffer a lateral compression larger than 0.5%. The transition does not appear in the Ho–Zr multilayers; the steadily increasing magnetization measured under weak magnetic field (500 Oe) rather indicates that ferromagnetic ordering set in from 130 K. An additional illustration of the enhanced trend towards ferromagnetism is given by the behaviour of the critical field H_c measured at various temperatures in the Ho30–Zr30 multilayer. Above 20 K, the values of H_c stand well below the values measured for bulk Ho and approach those reported for Ho–Lu superlattices.

Another interesting feature of the Ho–Zr superlattices investigated is the existence of an oscillatory magnetic coupling between Ho layers when the thickness of the non-magnetic Zr spacer is changed. Following the results recently reported for Ho–Sc superlattices [31], this is new evidence for the existence of interlayer coupling in RE–M superlattices characterized by a large lattice misfit between the two metals. No evidence of such an interlayer magnetic interaction was noted for other RE–Zr superlattices (RE = Dy, Tm) developed under the same conditions [8, 12]. The difference between the behaviours observed in the Dy–Zr and Ho–Zr superlattices could result from differences in the Fermi surfaces of Dy and Ho. In addition, the structure of RE–Zr interfaces should be considered owing to the dependence of the amplitude of the interlayer coupling oscillations on the existence of interfacial defects. A qualitative picture of this coupling is that ferromagnetic order in the Ho layers propagates through the non-magnetic metal in such a way that the magnetization is the result of either constructive or destructive interference, leading thus to the oscillations observed in the squareness of the hysteresis loops as the thickness of the Zr layers changes. A possible mechanism for this propagation is that it takes place via a polarization of the conduction electrons giving rise to a spin-density wave in the non-magnetic spacer layer. On the other hand, the existence of a large concentration of defects and roughness at the interfaces generates destructive interference which contributes to the blurring of the coupling oscillations. Then, a larger interfacial roughness could explain the absence of interlayer coupling in the Dy–Zr superlattices previously investigated by our group.

Finally, it appears that Ho–Zr interfaces generate an out-of-plane contribution to magnetic anisotropy in the Ho(x Å)–Zr(30 Å) multilayers. The interface anisotropy is oriented perpendicular to the basal plane of the hcp structure. It increases as the Ho layers become thinner and is strong enough to compensate the in-plane volume anisotropy for Ho layers of $\approx$7 Å, i.e. three monolayers. Notwithstanding a rather large scattering in the experimental values, it may be reasonably claimed that the dependence of the magnetic anisotropy on the thickness of

Ho layers follows the prediction of the crystal-field model using the screened point-charge approximation. The same agreement was previously observed for Dy–Zr superlattices. The ability of the oversimplified point-charge version of the crystal-field model to reproduce the data may be interestingly compared to the good agreement between the magnetic anisotropies calculated from this model and the experimental values deduced from the paramagnetic Curie temperatures measured for the heavy rare earths with the applied magnetic field parallel and perpendicular to the basal plane of the hcp structure [32].

References

[1] Salamon M B, Sinha S, Rhyne J J, Cunningham J E, Erwin R W, Borchers J and Flynn C P 1986 *Phys. Rev. Lett.* **56** 259
[2] Erwin R W, Rhyne J J, Salamon M B, Borchers J, Sinha S, Du R, Cunningham J E and Flynn C P 1987 *Phys. Rev.* B **35** 6808
[3] Beach R S, Borchers J, Matheny A, Erwin R W, Salamon M B, Everitt B, Pettit K, Rhyne J J and Flynn C P 1993 *Phys. Rev. Lett.* **70** 3502
[4] Tsui F and Flynn C P 1993 *Phys. Rev. Lett.* **71** 1462
[5] Erwin R W, Rhyne J J, Borchers J, Salamon M B, Du R and Flynn C P 1988 *J. Appl. Phys.* **63** 3461
[6] Jehan D A, McMorrow D F, Cowley R A, Ward R C C, Wells M R and Hagmann N 1993 *Phys. Rev.* B **48** 5594
[7] Swaddling P P, McMorrow D F, Cowley R A, Simpson J A, Wells M R, Ward R C C, Clausen K N, Collins M F and Buyers W J L 1995 *J. Magn. Magn. Mater.* **140–144** 783
[8] Baudry A, Boyer P and Brunel M 1998 *J. Magn. Magn. Mater.* **185** 309
[9] Bohr J, Gibbs D, Axe J D, Moncton D E, d'Amico K L, Majkrzak C F, Kwo J, Hong M, Chien C L and Jensen J 1989 *Physica* B **159** 93
[10] Rhyne J J, Erwin R W, Borchers J, Salamon M B, Du R and Flynn C P 1989 *Physica* B **159** 111
[11] Raquet B, Sdaq A, Broto J M, Rakoto H, Ousset J C, Askenazy S, Baudry A, Boyer P, Luche M C and Khmou A 1995 *Physica* B **211** 335
[12] Luche M C, Baudry A, Boyer P, Rouviere J L, Fermon C and Miramond C 1995 *J. Magn. Magn. Mater.* **150** 175
[13] Tomka G J, de Groot P A J, Rainford B D, Wells M R, Ward R C C and del Moral A 1995 *J. Magn. Magn. Mater.* **140–144** 777
[14] Tomka G J, de Groot P A J, Rainford B D, Wells M R, Ward R C C and Arnaudas J I 1995 *J. Magn. Magn. Mater.* **140–144** 785
[15] Jensen J and Mackintosh A R 1991 *Rare Earth Magnetism* (Oxford: Clarendon)
[16] Arnaudas J I, del Moral A, Ciria M, Tomka G J, de la Fuente C, de Groot P A J, Ward R C C and Wells M R 1996 *J. Magn. Magn. Mater.* **156** 421
[17] Luche M C 1993 *PhD Thesis* Grenoble University
[18] Locquet J P, Neerinck D, Stockman L, Bruynseraede Y and Schuller I K 1988 *Phys. Rev.* B **38** 3572
[19] Bruno P and Renard J P 1989 *Appl. Phys.* A **49** 499
[20] Scott T E 1978 *Handbook on the Physics and Chemistry of Rare Earths* vol 1 (Amsterdam: North-Holland) p 686
[21] Bartholin H, Beille J, Bloch D, Boutron P and Féron J L 1979 *J. Appl. Phys.* **42** 1679
[22] Cooper B R 1968 *Solid State Physics* vol 21, ed F Seitz, D Turnbull and H Ehrenreich (New York: Academic) p 393
[23] Strandburg D L, Legvold S and Spedding F H 1962 *Phys. Rev.* **127** 2046
[24] Ousset J C 1993 personal communication
[25] Féron J L 1969 *Phd Thesis* Grenoble University
[26] Kwo J, Hong M, di Salvo F J, Waszczak J V and Majkrzak C F 1987 *Phys. Rev.* B **35** 7295
[27] Yafet Y 1987 *J. Appl. Phys.* **61** 4058
[28] Deaven D M, Rokhsar D S and Johnson M 1991 *Phys. Rev.* B **44** 5977
[29] Bruno P and Chappert C 1991 *Phys. Rev. Lett.* **67** 1602
[30] Bruno P and Chappert C 1992 *Phys. Rev.* B **46** 261
[31] Bryn-Jacobsen C, Cowley R A, McMorrow D F, Goff J P, Ward R C C and Wells M R 1997 *Phys. Rev.* B **55** 317
[32] Coqblin B 1977 *The Electronic Structure of Rare-Earth Metals and Alloys: the Magnetic Heavy Rare-Earths* (London: Academic) p 198, and references therein
[33] Vianden R 1987 *Hyperfine Interact.* **35** 1079
[34] Buschow K H J 1977 *Rep. Prog. Phys.* **40** 1179